ORNL/TM-2014/316

Oak Ridge National Laboratory Sensitivity Analysis of X-ray Spectra from Scanning Electron Microscopes

Thomas M. Miller
Bruce W. Patton
Charles F. Weber
Kursat B. Bekar

October 16, 2014

OAK RIDGE NATIONAL LABORATORY
MANAGED BY UT-BATTELLE FOR THE US DEPARTMENT OF ENERGY

ORNL/TM-2014/316

Reactor and Nuclear Systems Division

SENSITIVITY ANALYSIS OF X-RAY SPECTRA FROM SCANNING ELECTRON MICROSCOPES

Report for Office of Defense Nuclear Nonproliferation Research and Development (DNN R&D) Project OR13-SEMS045-PD3TB

Thomas M. Miller
Bruce W. Patton
Charles F. Weber
Kursat B. Bekar

Date Published: October 2014

Prepared by
OAK RIDGE NATIONAL LABORATORY
Oak Ridge, Tennessee 37831-6283
managed by
UT-BATTELLE, LLC
for the
US DEPARTMENT OF ENERGY
under contract DE-AC05-00OR22725

CONTENTS

LIST OF FIGURES

LIST OF TABLES

ACRONYMS

ASCII	American Standard Code for Information Interchange
DNN	Office of Defense Nuclear Nonproliferation Research and Development
DOE	Department of Energy
IAEA	International Atomic Energy Agency
KUT	potassium, uranium, and thorium
NORM	naturally occurring radioactive material
ORNL	Oak Ridge National Laboratory
PENELOPE	Penetration and Energy Loss of Positrons and Electrons
R&D	research and development
SEM	scanning electron microscope
UNSCEAR	United Nations Scientific Committee on the Effects of Atomic Radiation

1. INTRODUCTION

The primary goal of this project is to evaluate x-ray spectra generated within a scanning electron microscope (SEM) to determine elemental composition of small samples. This will be accomplished by performing Monte Carlo simulations of the electron and photon interactions in the sample and in the x-ray detector. The elemental inventories will be determined by an inverse process that progressively reduces the difference between the measured and simulated x-ray spectra by iteratively adjusting composition and geometric variables in the computational model. The intended benefit of this work will be to develop a method to perform quantitative analysis on substandard samples (heterogeneous phases, rough surfaces, small sizes, etc.) without involving standard elemental samples or empirical matrix corrections (i.e., true standardless quantitative analysis).

To distinguish samples containing different elemental components, it is necessary for some spectral features to be different. If two samples of different compositions have identical spectra, then it is impossible to distinguish those samples using x-ray spectra alone. Thus, a sensitivity analysis can be used to identify areas where the spectra are useful for identification and where they are not. Sensitivity analysis can also be used to assign uncertainty to elemental assessments, to understand where atomic-interaction data are deficient, and to identify cases where additional information is required.

A sensitivity analysis identifies geometric features that can impact measured x-ray spectra. Information about the geometry of the sample can be gained from the images created by the SEM. These images are actually the primary purpose of an SEM. However, the SEM's imaging capability does not have infinite resolution, and the images generated only represent the surface of a sample. Therefore, a sensitivity analysis will help determine what geometric features impact the measured x-ray spectra and what geometric features can be ignored because they do not impact the x-ray spectra.

This report evaluates the sensitivity of SEM x-ray spectra to changes in a number of different parameters, as listed in Table 1.

Table 1. Parameters investigated during sensitivity analysis

Composition dependent	**Geometric dependent**
1) Material composition	1) Surface roughness
2) Material density	2) Material heterogeneity (inclusions)
3) Material stopping power	
4) Electron shell transition probabilities	

About half of the quantities in Table 1 will be evaluated by calculating a sensitivity coefficient (material density, material stopping power, and electron shell transition probabilities). The absolute sensitivity, S_{abs}, is determined by calculating the change in a dependent variable, Y (number of x-rays of a given energy), relative to the change in an independent variable, X.

$$S_{abs} = \frac{Y_1 - Y_2}{X_1 - X_2} = \frac{\Delta Y}{\Delta X}$$

The relative sensitivity, S_{rel}, is the absolute sensitivity relative to the nominal values of the independent variable and dependent variable (or the fractional change in Y per the fractional change in X).

$$S_{rel} = \frac{\Delta Y / Y}{\Delta X / X}$$

This relative sensitivity is what is known as the sensitivity coefficient. The sensitivities presented in this report were calculated using the expression for S_{rel}, so they are sensitivity coefficients. In all cases, the independent variable, X, was changed by ±10%, and the corresponding change in the dependent variable, Y, was calculated. These three data points (X - 10%, X, and X + 10%) were used to calculate the sensitivity coefficients and to ensure that each perturbation was linear. Independent variables of composition and density were changed when mixing the cross sections for the simulations. The stopping power and electron shell transition probabilities were changed by modifying the ASCII file containing the "mixed" macroscopic cross section data. Perturbations of surface roughness and heterogeneity were performed by changing the geometry.

Sensitivity coefficients will not be reported for the remaining items in Table 1 (material composition, surface roughness, and material heterogeneity). Rather, they will be evaluated quantitatively. For example, it will be determined whether statistically different x-ray spectra can be calculated for samples with different compositions or whether surface roughness has a statistically significant impact on the simulated x-ray spectrum.

Previous tasks on this project have focused on development of an effective Monte Carlo computational tool for SEM simulations [1,2]. Several existing codes were examined and compared in terms of accuracy, code performance, and the capabilities to simulate the physics in the SEM process at the level of detail required for this project. PENELOPE [3] was selected as the particle transport code for detailed SEM simulations from all the available candidates. One of the significant benefits of PENELOPE is its relatively short computational time compared to the other candidate detailed electron/photon transport codes. This is because of its advanced CLASS-II algorithm for electron transport, which is a combination of single event and condensed history transport algorithms.

However, because PENELOPE is serial, it slows down SEM simulations due to the lack of high performance computing capability. Therefore, the Oak Ridge National Laboratory (ORNL) developed a high performance version of PENELOPE, penORNL [4]. penORNL was developed in a modular structure relying on the original PENELOPE functions and subroutines. The modular structure enables easy replacement of one of its modules with another one depending on the requirements in the simulations. For example, the geometry module can be replaced with an advanced geometry module to support very complex geometries. A scanning source capability has been integrated into penORNL to simulate the raster pattern of an SEM. In the SEM process, the Si-drift-based detector is a pulse-height detector which counts the number of pulses of different amounts of energy deposited in the detector crystal. In order to simulate this type of detector more realistically, a pulse-height tally feature has been added to the new tally module. In this implementation, the pulse-height tally bins represent different amounts of energy deposited, as in a pulse-height detector. The parallel performance of penORNL was extensively tested with several model problems, and linear parallel scaling was observed with the number of processors (speedup of 501 with 512 processors).

2. SENSITIVITY EVALUATION OF COMPOSITION DEPENDENT PARAMETERS

The analysis evaluated the sensitivity of x-ray spectra to the elemental composition and related parameters such as density, material stopping power, and electron shell transition probabilities. The density and composition varied from sample to sample, but the last two quantities are basic physical properties of the elements, which should be constant between samples.

2.1. MATERIAL COMPOSITION

In this case, no sensitivity coefficients are presented because the independent variable *X* is the material composition, not a numerical value such as density or stopping power. Therefore, only a difference in the number of x-rays produced or the observation of different characteristic x-ray energies can be considered. X-ray spectra for different compositions are presented in the following figures, along with a comparison of the number of x-rays for some select characteristic x-ray energies in the following tables. These calculations were performed with 15, 25, and 35 keV electron beams. The materials considered in this evaluation are focused on the uranium compounds listed in Table 2. Figure 1 compares the characteristic x-ray spectra for samples of pure metallic U and UN (each 2 μm thick) created by a 25 keV electron beam. Figure 2 shows the ratio of the U and UN spectra. These two materials are very similar when one considers the electrons present in the sample, and their densities are also fairly similar (U 19.1 g/cm^3 and UN 14.31 g/cm^3). The x-ray lines in Figure 1 all occur at identical energies. The additional lines created by N in UN do not appear because they all occur below 1 keV, which is the lower limit of the data tallied in this evaluation. A measurement of these spectra would show the additional nitrogen lines distinguishing the two materials. Therefore, transport below 1 keV should be evaluated further for future analysis. The difference in the magnitude of the spectra is due to the difference in density, as the higher-density U sample generates a larger number of x-rays. As Figure 1 and Figure 2 suggest, it is difficult to distinguish compounds with very similar elemental compositions and mass densities, but it is not impossible.

Table 2. Uranium compounds considered in sensitivity analysis

1)	U (metal)	9)	UC
2)	U_3O_8	10)	UC_2
3)	UO_2	11)	UO_2F_2
4)	UO_3	12)	$UO_2(NO_3)_2$
5)	UF_4	13)	UH_3
6)	UF_6	14)	UO_2SO_4
7)	UN	15)	Zippeite - $K_4(UO_2)_6(SO_4)_3(OH)_{10}\cdot 4H_2O$
8)	UCl_4	16)	Johannite - $Cu[UO_2(OH)SO_4]_2\cdot 8H_2O$

A second comparison with a 25 keV electron beam is shown in Figure 3 and Figure 4 for UF_6 and Johannite (a copper-uranyl sulfate mineral), which are uranium compounds with very different secondary elements. The most obvious difference is in the magnitude of the spectra. Since UF_6 has a larger mass density than Johannite (5.09 g/cm^3 versus 3.32 g/cm^3) and a larger density of uranium atoms and electrons (8.708×10^{21} atoms/cm^3 versus 4.106×10^{21} atoms/cm^3), the UF_6 sample produces more x-rays. The x-rays generated by F in UF_6 are all below 1 keV, which is similar to nitrogen as shown in Figure 1. However, the Johannite sample produces a few x-ray lines above 1 keV that are different than those produced by U. These additional lines are produced by Cu (near 1, 8, and 8.9 keV) and S (near 2.3 keV), and they clearly stand out in the Figure 4 ratio plot.

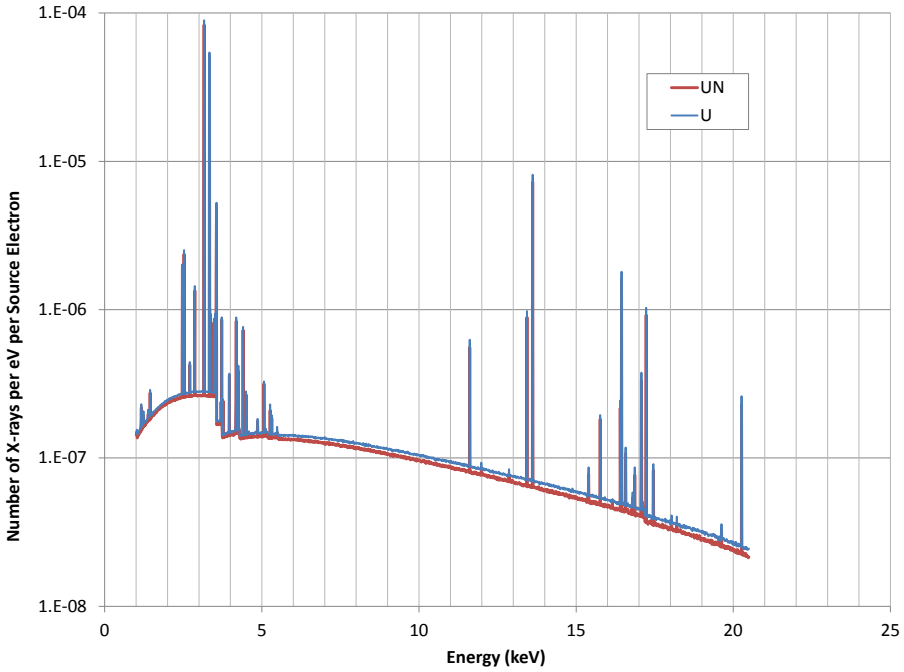

Figure 1. Comparison of the characteristic x-ray spectra generated by U and UN with a 25 keV electron beam.

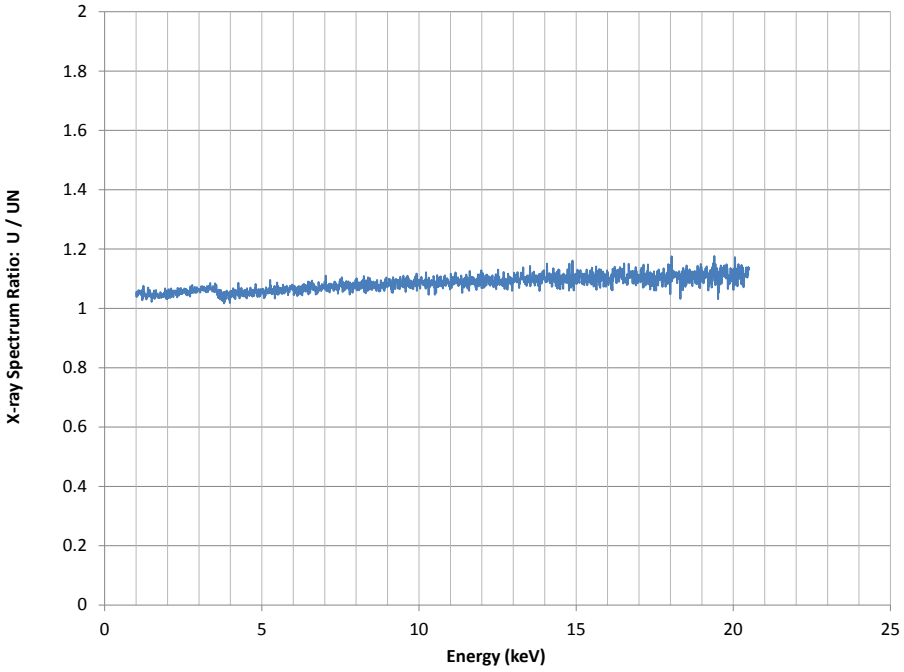

Figure 2. Ratio of x-ray spectra generated by U and UN with a 25 keV electron beam.

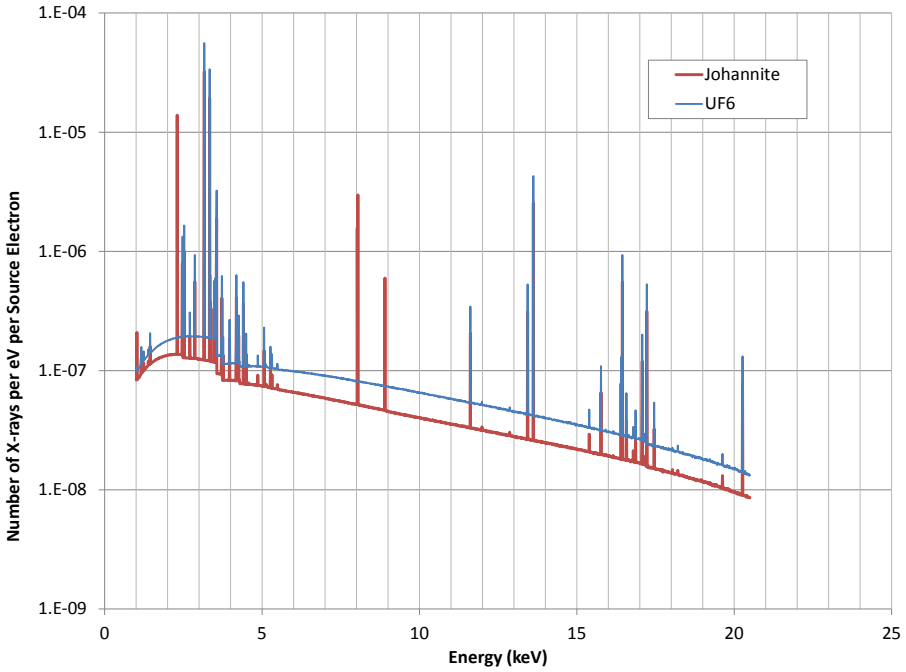

Figure 3. Comparison of the characteristic x-ray spectra generated by UF_6 and Johannite with a 25 keV electron beam.

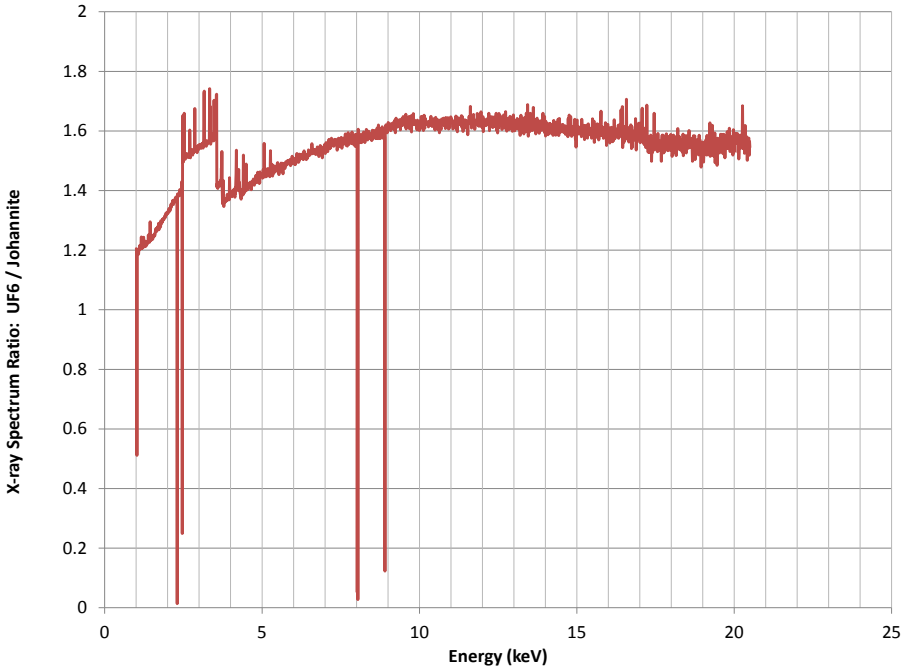

Figure 4. Ratio of x-ray spectra generated by UF_6 and Johannite with a 25 keV electron beam.

To aid the comparison of data presented in Figure 1 through Figure 4, a few of the more prominent x-ray lines for U have been selected, and the numbers of x-rays at these energies have been plotted in Figure 5 and Figure 6. Table 3, Table 4, and Table 5 list the numerical differences between the numbers of these

prominent U characteristic x-rays generated by 15, 25, and 35 keV electron beams, respectively. These tables also include the percentage difference and the uncertainty of the calculated difference in percent. Table 4 lists the numerical differences between the data points plotted in Figure 5 and Figure 6. The calculated differences between the U and UN spectra are very small (~10% or less), and the uncertainties on some of the calculated differences are larger than the calculated differences. For U and UN in Table 4, the calculated difference in the x-ray spectra at 11.62 and 17.23 keV is about 10% of the U spectrum, but the uncertainty is large—28% and 23% (2 sigma), respectively. These large uncertainties indicate that the calculated differences are not statistically significant. However, if even a single peak (or bin) in the spectra exhibit statistically significant differences, it likely will be possible to distinguish the materials. On the other hand, the calculated differences between UF_6 and Johannite in Table 4 are large and statistically significant. Again, the results of this comparison show that similar materials have much smaller differences in the characteristic x-ray spectra. In other words, materials with similar densities and similar chemical compositions (e.g., U and UN) produce about the same number of x-rays for a given characteristic x-ray energy, which is a well-known fact. On the other hand, materials that are different will produce different numbers of x-rays for a given characteristic x-ray energy, and more importantly (as seen in Figure 3), they will produce x-rays at different energies.

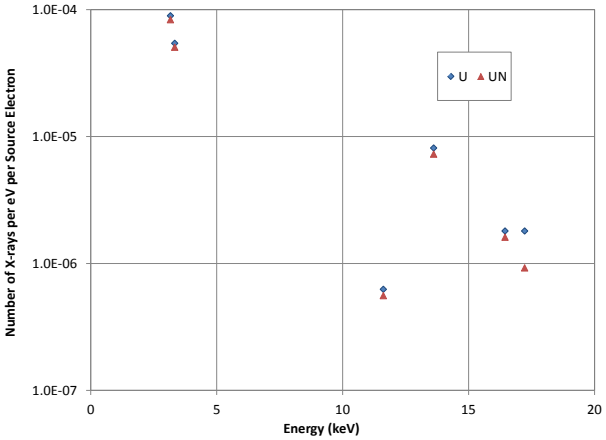

Figure 5. Comparison of number of select characteristic x-rays generated by U and UN for a 25 keV electron beam.

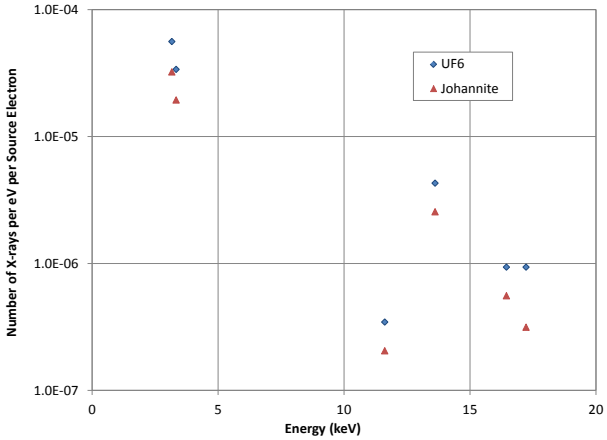

Figure 6. Comparison of number of select characteristic x-rays generated by UF_6 and Johannite for a 25 keV electron beam.

Table 3. Comparison of the number of characteristic x-rays for a 15 keV electron beam

X-ray energy (keV)	3.165	3.335	11.62	13.62
*Δ = U – UN	4.390E-06	2.588E-06	3.160E-09	1.767E-09
% Difference	8.26%	8.28%	9.66%	11.71%
Δ Relative uncertainty (%)	1.53%	1.99%	12.78%	15.45%
*Δ = UF_6 – Johannite	1.160E-05	6.784E-06	6.221E-09	2.862E-09
% Difference	36.06%	36.03%	33.93%	37.84%
Δ Relative uncertainty (%)	0.21%	0.27%	2.37%	3.29%

*Units are x-rays per eV per source electron

Table 4. Comparison of the number of characteristic x-rays for a 25 keV electron beam

X-ray energy (keV)	3.165	3.335	11.62	13.62	16.45	17.23
*Δ = U – UN	6.130E-06	3.732E-06	6.717E-08	8.620E-07	1.935E-07	1.074E-07
% Difference	6.86%	6.88%	10.75%	10.61%	10.73%	10.44%
Δ Relative uncertainty (%)	2.10%	2.68%	14.15%	4.25%	8.80%	11.86%
*Δ = UF_6 – Johannite	2.368E-05	1.439E-05	1.405E-07	1.735E-06	3.779E-07	2.159E-07
% Difference	42.30%	42.60%	40.69%	40.48%	40.44%	40.69%
Δ Relative uncertainty (%)	0.19%	0.25%	2.35%	0.72%	1.53%	2.00%

*Units are x-rays per eV per source electron

Table 5. Comparison of number of characteristic x-rays for a 35 keV electron beam

X-ray **e**nergy (keV)	3.165	3.335	11.62	13.62	16.45	17.23
*Δ = U – UN	6.125E-06	4.289E-06	2.053E-07	2.801E-06	6.836E-07	6.658E-07
% Difference	5.67%	6.36%	10.40%	9.95%	10.77%	10.02%
Δ Relative uncertainty (%)	3.12%	3.51%	11.55%	3.29%	6.35%	6.66%
*Δ = UF_6 – Johannite	3.052E-05	1.879E-05	4.847E-07	6.883E-06	1.526E-06	1.616E-06
% Difference	52.77%	53.15%	50.96%	51.63%	52.21%	49.37%
Δ Relative uncertainty (%)	0.15%	0.19%	1.16%	0.31%	0.66%	0.66%

*Units are x-rays per eV per source electron

There is another interesting trend in Table 3 through Table 5 that is worthy of discussion. If the comparisons between UF_6 and Johannite are considered alone, one might conclude that increasing the energy of the electron beam is always beneficial for distinguishing similar x-ray spectra. This is because the percent difference of the number of x-rays generated is increasing as the electron energy increases. However, the comparison between U and UN alone would not likely lead to this same conclusion. In this case, the percent difference decreases or is about the same for increasing electron energy. Furthermore, for the U and UN comparison, the most statistically meaningful data are for the two characteristic x-rays around 3 keV when the electron beam energy is 15 keV.

2.2. MATERIAL MASS DENSITY

Using the same materials and characteristic x-ray energies used in Section 2.1, the sensitivity with respect to mass density was evaluated for 15, 25, and 35 keV SEM electrons. For the 2 μm-thick samples, the x-ray spectrum was not sensitive to density for several of the materials evaluated. In fact, almost none of the x-ray spectra were sensitive to density for a 15 keV electron beam. In general, the x-ray spectrum was not sensitive to density if the sample thickness was larger than the size of the interaction volume in the sample, which is related to and usually slightly larger than the range of the SEM electron in that sample. For this evaluation, if the range was less than ~2 – 4 μm, the x-ray spectrum was not sensitive to density. This corresponds to the well-known fact that SEM images only contain data where the interaction volume was within the sample, which usually corresponds to the outer surface of a sample. Once the thickness of a sample becomes greater than the size of the interaction volume (approximately the range of SEM electrons in the sample), then there are parts of the sample that cannot be imaged, and the x-ray spectrum created by SEM electrons in the sample is not sensitive to the sample density. Table 6 lists some of the materials from Table 2, along with their electron ranges for the energies used in this evaluation.

Table 6. Example electron ranges as a function of electron energy

Compound	Density (g/cm^3)	15 keV Range (μm)	25 keV Range (μm)	35 keV Range (μm)
U (metal)	19.1	0.84	1.84	3.14
UC_2	11.28	1.27	2.84	4.88
UF_6	5.09	2.17	5.06	8.89
$UO_2(NO_3)_2$	2.81	3.49	8.23	14.54

Table 7 through Table 9 present the sensitivity coefficients calculated by this evaluation. Notice that the sensitivity to density increases with increasing electron beam energy, which corresponds to increasing interaction volume size. Some sensitivity values in Table 7 through Table 9 are listed as N/A. These represent differences in the number of characteristic x-rays (ΔY) not statistically different on the 95% confidence interval (2-sigma). If a uranium compound listed in Table 2 is not present in Table 7 through Table 9, then there was no sensitivity to density for that material. This same notation will be used for the remainder of Section 2.

Table 7. Sensitivity coefficient of x-ray spectra to density for a 15 keV electron beam

Material	Nominal density (g/cm^3)	Characteristic x-ray energies (keV)	
		3.165	3.335
$UO_2(NO_3)_2$	2.81	0.057	0.064

Table 8. Sensitivity coefficient of x-ray spectra to density for a 25 keV electron beam

Material	Nominal density (g/cm^3)	Characteristic x-ray energies (keV)					
		3.165	3.335	11.62	13.62	16.45	17.23
UF_6	5.09	0.188	0.195	N/A	N/A	N/A	N/A
UCl_4	4.87	0.158	0.163	N/A	N/A	N/A	N/A
UO_2F_2	6.37	0.059	N/A	N/A	N/A	N/A	N/A
$UO_2(NO_3)_2$	2.81	0.793	0.799	0.501	0.378	0.404	N/A
UO_2SO_4	3.28	0.594	0.606	0.387	0.255	N/A	N/A
Zippeite	3.66	0.463	0.492	N/A	0.220	N/A	N/A
Johannite	3.32	0.566	0.577	N/A	0.209	N/A	N/A

Table 9. Sensitivity coefficient of x-ray spectra to density for a 35 keV electron beam

Material	Nominal density (g/cm^3)	Characteristic x-ray energies (keV)					
		3.165	3.335	11.62	13.62	16.45	17.23
U_3O_8	8.30	0.174	0.201	N/A	0.191	N/A	N/A
UO_3	7.29	0.287	0.298	N/A	0.282	0.278	N/A
UF_4	6.70	0.381	0.401	0.407	0.349	0.382	0.223
UF_6	5.09	0.694	0.712	0.517	0.573	0.575	0.468
UCl_4	4.87	0.616	0.644	0.541	0.594	0.638	0.451
UC_2	11.28	N/A	0.067	N/A	N/A	N/A	N/A
UO_2F_2	6.37	0.431	0.447	N/A	0.362	0.396	0.320
$UO_2(NO_3)_2$	2.81	1.166	1.176	1.074	1.058	1.067	0.933
UO_2SO_4	3.28	1.055	1.078	0.989	0.955	0.967	0.819
Zippeite	3.66	0.997	1.016	0.843	0.858	0.871	0.740
Johannite	3.32	1.057	1.089	0.958	0.922	0.895	0.824

2.3. MATERIAL STOPPING POWER

Bethe described the rate of energy loss, *dE* (keV) of an electron per the distance traveled, *ds* (μm), as

$$\frac{dE}{ds} = -2\pi e^4 N_o \frac{Z\rho}{AE_i} \ln\left(\frac{1.166E_i}{J}\right),$$

where *e* is the electron charge, N_o is Avogadro's number, *Z* is the atomic number, ρ is the density, *A* is the atomic weight, E_i is the electron energy, and *J* is the average energy loss per electron collision with element *Z* [5]. For electron calculations, the concept of the stopping power, *S*, of the target is used frequently, which is defined as the rate of energy loss per unit path length divided by the density ρ. Hence,

$$S = -\frac{1}{\rho}\frac{dE}{ds}$$

in which the Bethe formulation is used for the rate of energy loss. The higher the stopping power, the more quickly the electrons lose their energy in the medium, and hence the depth of penetration will be less. The stopping power is not a parameter that can or should be modified in simulation input. Rather, it is considered basic data that are provided to a radiation transport code which in turn uses it to simulate the electron and photon transport. Large sensitive coefficients to stopping power indicate how important that parameter is to solving this problem and how important it is to have accurate stopping power data.

The sensitivity analysis performed for density was repeated for stopping power. The results of this analysis are shown in Table 10 through Table 12. One can see that the sensitivity for a given characteristic x-ray energy is similar between the different U compounds that were evaluated, with only a few exceptions. This suggests that the variation between different compositions and densities is small and that stopping power sensitivity and uncertainties will not vary greatly between different compounds. Notice that nearly all of these sensitivity coefficients are negative, which means the number of characteristic x-rays produced will decrease with an increase in the material stopping power.

Table 10. Sensitivity coefficient of x-ray spectra to stopping power for a 15 keV electron beam

Material	Stopping power (keV/μm)	Characteristic x-ray energies (keV)			
		3.165	3.335	11.62	13.62
U	12.45	-0.61	-0.61	N/A	N/A
U_3O_8	6.38	-0.64	-0.65	N/A	N/A
UO_2	8.15	-0.65	-0.64	N/A	N/A
UO_3	5.69	-0.65	-0.66	N/A	N/A
UF_4	5.41	-0.66	-0.67	N/A	N/A
UF_6	4.38	-0.68	-0.68	N/A	N/A
UN	9.97	-0.61	-0.63	N/A	N/A
UCl_4	4.18	-0.64	-0.64	N/A	N/A
UC	9.42	-0.62	-0.62	N/A	N/A
UC_2	8.19	-0.63	-0.64	N/A	N/A
UO_2F_2	5.16	-0.66	-0.67	N/A	N/A
$UO_2(NO_3)_2$	2.69	-0.67	-0.69	N/A	N/A
UH_3	7.66	-0.61	-0.62	N/A	N/A
UO_2SO_4	2.97	-0.67	-0.69	N/A	N/A
Zippeite	3.44	-0.70	-0.70	N/A	N/A
Johannite	3.48	-0.72	-0.72	N/A	N/A

Table 11. Sensitivity coefficient of x-ray spectra to stopping power for a 25 keV electron beam

Material	Stopping power (keV/μm)	Characteristic x-ray energies (keV)					
		3.165	3.335	11.62	13.62	16.45	17.23
U	8.83	-0.49	-0.51	N/A	-0.67	-0.75	-0.78
U_3O_8	4.47	-0.52	-0.55	-0.65	-0.73	-0.70	-0.75
UO_2	5.73	-0.53	-0.53	N/A	-0.68	-0.73	-0.73
UO_3	3.99	-0.52	-0.55	-0.71	-0.71	-0.77	-0.90
UF_4	3.78	-0.53	-0.53	-0.71	-0.77	-0.74	-0.74
UF_6	3.05	-0.47	-0.48	-0.62	-0.78	-0.72	-0.80
UN	7.03	-0.52	-0.52	N/A	-0.75	-0.69	-0.71
UCl_4	2.91	-0.42	-0.43	-0.59	-0.77	-0.70	-0.78
UC	6.65	-0.50	-0.52	-0.63	-0.71	-0.68	-0.71
UC_2	5.76	-0.52	-0.54	-0.73	-0.75	-0.70	-0.80
UO_2F_2	3.61	-0.51	-0.53	-0.56	-0.75	-0.79	-0.77
$UO_2(NO_3)_2$	1.86	-0.17	-0.18	-0.45	-0.62	-0.59	-0.71
UH_3	5.41	-0.49	-0.50	N/A	-0.70	-0.75	-0.78
UO_2SO_4	2.06	-0.25	-0.25	N/A	-0.68	-0.65	-0.74
Zippeite	2.38	-0.33	-0.34	-0.65	-0.72	-0.70	-0.83
Johannite	2.39	-0.31	-0.30	-0.46	-0.71	-0.70	-0.82

Table 12. Sensitivity coefficient of x-ray spectra to stopping power for a 35 keV electron beam

Material	Stopping power (keV/μm)	Characteristic x-ray energies (keV)					
		3.165	3.335	11.62	13.62	16.45	17.23
U	7.06	-0.42	-0.44	N/A	-0.57	-0.50	-0.48
U_3O_8	3.55	-0.37	-0.36	-0.55	-0.58	-0.58	-0.54
UO_2	4.55	-0.41	-0.43	-0.55	-0.62	-0.64	-0.63
UO_3	3.16	-0.32	-0.32	-0.47	-0.55	-0.57	-0.57
UF_4	2.99	-0.27	-0.28	-0.46	-0.55	-0.46	-0.55
UF_6	2.40	-0.13	-0.11	-0.28	-0.43	-0.42	-0.50
UN	5.61	-0.42	-0.44	N/A	-0.64	-0.61	-0.60
UCl_4	2.30	-0.10	-0.11	-0.34	-0.37	-0.35	-0.46
UC	5.30	-0.40	-0.40	N/A	-0.61	-0.61	-0.58
UC_2	4.58	-0.41	-0.42	-0.55	-0.67	-0.68	-0.56
UO_2F_2	2.85	-0.24	-0.26	-0.50	-0.49	-0.53	-0.55
$UO_2(NO_3)_2$	1.46	0.07	0.08	N/A	-0.16	N/A	-0.22
UH_3	4.31	-0.41	-0.42	-0.54	-0.59	-0.58	-0.64
UO_2SO_4	1.62	0.05	N/A	N/A	-0.21	-0.16	-0.26
Zippeite	1.87	N/A	N/A	N/A	-0.26	-0.23	-0.35
Johannite	1.87	0.03	N/A	N/A	-0.23	-0.16	-0.31

2.4. ELECTRON SHELL TRANSITION PROBABILITIES

When a source electron or photon collides with an orbital electron in the sample and removes that orbital electron, then electrons from outer shells will drop into lower shells to replace the missing electron. This process can often create a cascade of electrons dropping to lower shells, particularly for high-Z elements. As electrons transition to different shells, fluorescent photons (x-rays) with characteristic energies are produced. Each possible transition is based on allowable transitions between different electron energies and is given a probability based on measurements and theory. Like stopping power, electron shell

transition probabilities are inherent qualities of the elements present and are therefore not subject to adjustment from one problem to the next. Thus, they are basic data provided to the radiation transport code, and this analysis is determining how sensitive x-ray spectra are to this basic data. Large sensitivity coefficients indicate that these data are important, and useful future work would include reducing the uncertainty of transition probabilities in order to reduce the uncertainties of the simulated x-ray spectra.

A sensitivity analysis for transition probabilities was performed that was very similar to that performed for mass density and stopping power. The results of this analysis are shown in Table 13 through Table 15. Like the stopping power sensitivities, these sensitivities are very similar for a given characteristic x-ray energy, so the variations due to changes in material composition and density are small. The sensitivity for the lower energy x-rays (~3 keV) are fairly large compared to most of the other sensitivities presented in this evaluation. This suggests that transition probabilities are one of the more important parameters considered so far.

Table 13. Sensitivity coefficients of x-ray spectra to transition probabilities for a 15 keV electron beam

Material	Characteristic x-ray energies (keV)			
	3.165	3.335	11.62	13.62
	Transition probabilities—Nominal values			
	0.0734193	0.05427	0.0199593	0.2771379
U	0.93	0.93	N/A	N/A
U_3O_8	0.93	0.94	N/A	N/A
UO_2	0.94	0.94	N/A	N/A
UO_3	0.94	0.92	N/A	N/A
UF_4	0.93	0.93	N/A	N/A
UF_6	0.94	0.93	N/A	N/A
UN	0.94	0.93	N/A	N/A
UCl_4	0.94	0.93	N/A	N/A
UC	0.94	0.93	N/A	N/A
UC_2	0.94	0.92	N/A	N/A
UO_2F_2	0.94	0.94	N/A	N/A
$UO_2(NO_3)_2$	0.94	0.94	N/A	N/A
UH_3	0.93	0.93	N/A	N/A
UO_2SO_4	0.94	0.93	N/A	N/A
Zippeite	0.94	0.94	N/A	N/A
Johannite	0.94	0.93	N/A	N/A

Table 14. Sensitivity coefficients of x-ray spectra to transition probabilities for a 25 keV electron beam

Material	Characteristic x-ray energies (keV)					
	3.165	3.335	11.62	13.62	16.45	17.23
	Transition probabilities—-Nominal values					
	0.0734193	0.05427	0.0199593	0.2771379	0.0583803	0.3236589
U	0.93	0.97	N/A	0.60	0.59	0.73
U_3O_8	0.94	0.93	N/A	0.63	0.58	0.66
UO_2	0.94	0.93	N/A	0.61	0.59	0.72
UO_3	0.93	0.93	N/A	0.59	0.67	0.57
UF_4	0.93	0.94	N/A	0.58	0.57	N/A
UF_6	0.93	0.94	0.61	0.61	0.53	0.60
UN	0.94	0.94	N/A	0.61	0.64	0.65
UCl_4	0.93	0.92	N/A	0.59	0.57	0.56
UC	0.94	0.93	0.61	0.60	0.52	0.62
UC_2	0.94	0.95	N/A	0.61	0.56	0.63
UO_2F_2	0.94	0.93	0.58	0.60	0.60	0.69
$UO_2(NO_3)_2$	0.94	0.93	0.60	0.61	0.60	0.66
UH_3	0.94	0.93	0.55	0.58	0.57	0.66
UO_2SO_4	0.94	0.94	N/A	0.62	0.59	0.53
Zippeite	0.94	0.93	0.49	0.60	0.55	0.54
Johannite	0.94	0.94	0.47	0.58	0.57	0.60

Table 15. Sensitivity coefficients of x-ray spectra to transition probabilities for a 35 keV electron beam

Material	Characteristic x-ray energies (keV)					
	3.165	3.335	11.62	13.62	16.45	17.23
	Transition probabilities—Nominal values					
	0.0734193	0.05427	0.0199593	0.2771379	0.0583803	0.3236589
U	0.94	0.95	0.57	0.59	0.57	0.63
U_3O_8	0.93	0.93	0.56	0.61	0.56	0.62
UO_2	0.94	0.94	0.52	0.57	0.62	0.69
UO_3	0.94	0.92	0.57	0.58	0.53	0.65
UF_4	0.93	0.96	0.56	0.58	0.57	0.64
UF_6	0.94	0.94	0.55	0.60	0.59	0.63
UN	0.95	0.93	0.60	0.57	0.58	0.60
UCl_4	0.95	0.96	0.58	0.59	0.55	0.62
UC	0.93	0.93	0.63	0.59	0.59	0.60
UC_2	0.93	0.94	0.54	0.59	0.63	0.60
UO_2F_2	0.95	0.94	0.61	0.58	0.63	0.66
$UO_2(NO_3)_2$	0.94	0.93	0.52	0.59	0.62	0.64
UH_3	0.94	0.94	0.50	0.61	0.51	0.61
UO_2SO_4	0.94	0.93	0.57	0.59	0.54	0.65
Zippeite	0.94	0.93	0.56	0.60	0.58	0.67
Johannite	0.94	0.93	0.57	0.58	0.60	0.65

3. SENSITIVITY EVALUATION OF GEOMETRIC PARAMETERS

In order to use x-ray spectra to determine elemental and phase attributes of samples, it is necessary to understand the sensitivity of surface roughness and material heterogeneity on the computed spectra. Experiments have shown that surface roughness can affect the magnitude of the x-ray spectrum. Therefore, the inference of element mass present in the sample from spectrum peak magnitudes will have a larger uncertainty with increased sample surface roughness. Even with smooth surfaces, material heterogeneity will affect the spectrum based on the SEM electrons interacting with different material types. Small amounts of material buried deep within another material may be difficult or even impossible to detect. The spectrum will be dominated by the largest amount of material present, the material closest to the surface, and the material with the most direct line of sight to the x-ray detector (in the case of surface roughness). Therefore, materials with Z numbers very close to each other may be difficult to distinguish from one another.

3.1. SURFACE ROUGHNESS

It is well established in experimental SEM measurements that surface roughness plays an important role in the quality of the generated images. Great attention to detail is paid to sample polishing and preparation before analysis. Most SEM machines also have the ability to rotate the sample to mitigate these effects. Even though the focus is not on surface image generation, surface roughness affects the ability to detect underlying material. Since most SEM machines have only one detector, the roughness could shield x-rays depending on the detector's viewing angle. This is because the roughness could shield parts of the sample from the detector. Fortunately, the scanning nature of SEM machines will partially counteract this effect for material detection purposes. To discern the importance of surface roughness, a slab of pure uranium was modeled, and different pure uranium geometric shapes (e.g., cones, cubes, cuboidal ridges, hemispheres) of varying sizes were modeled on top of this slab. Since the cubes would provide the most self shielding of photons generated from electron interactions in the sample, it was determined to be the worst case of the different geometry types and will be focused on in this discussion. In an SEM machine, there is usually one detector that occupies only a small portion of the whole 2π hemisphere above the sample. Surface effects may reduce the photons seen by this detector. To determine the sensitivity of this effect, detectors were used for the whole 2π hemisphere and for the four quadrants of the hemisphere (denoted as Detectors 2–5). If the surface effects were large, the differences would be seen in the responses of the different detectors.

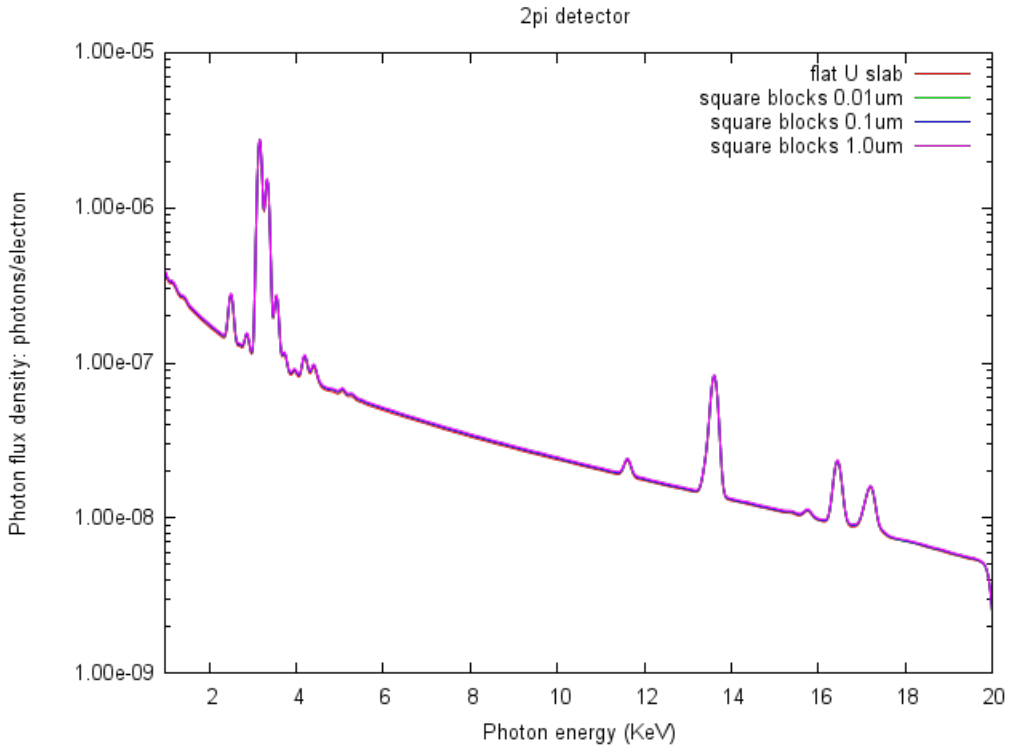

Figure 7. Surface geometry effects from a 2π detector viewpoint.

Figure 7 shows the x-ray spectrum from the uranium slab and differing heights of cubes of uranium on the slab as tallied on the large hemispherical (2π) detector. As expected, the differences are nonexistent, which, was expected for this idealized case.

Figure 8 through Figure 11 show the differences / sensitivity of the spectra on Detectors 2–5 located in the four quadrants of the hemisphere. While some effects are noted, most of the differences can be attributed to the statistics of the calculations, so the sensitivity of the detector response to geometry is minor. The lack of sensitivity is partly due to the scanning / raster nature of the electron beam in SEM machines, which is explicitly modeled in these penORNL simulations. A very fine scan over the surface will tend to evenly distribute the time the beam hits a valley (slab or uranium) and the time it hits the mountaintop (cube of uranium). Therefore, the overall effect is to average the differences expected to be seen from the different detectors. If the beam were held to a fixed point, then the detector response would be very dependent on hitting a cube or not. Therefore, the scanning nature of an SEM to create an image produces an average x-ray spectrum, obscuring the effect of surface roughness or heterogeneity on the computed detector response. However, the resulting SEM images can provide evidence of surface or material differences, which can prompt further investigation. This further investigation should use the ability of the SEM to control the beam energy, spot size, and scanning / raster area of the sample to generate a spectrum that is not an average of the bulk material, but rather the spectrum of a specific portion of the sample.

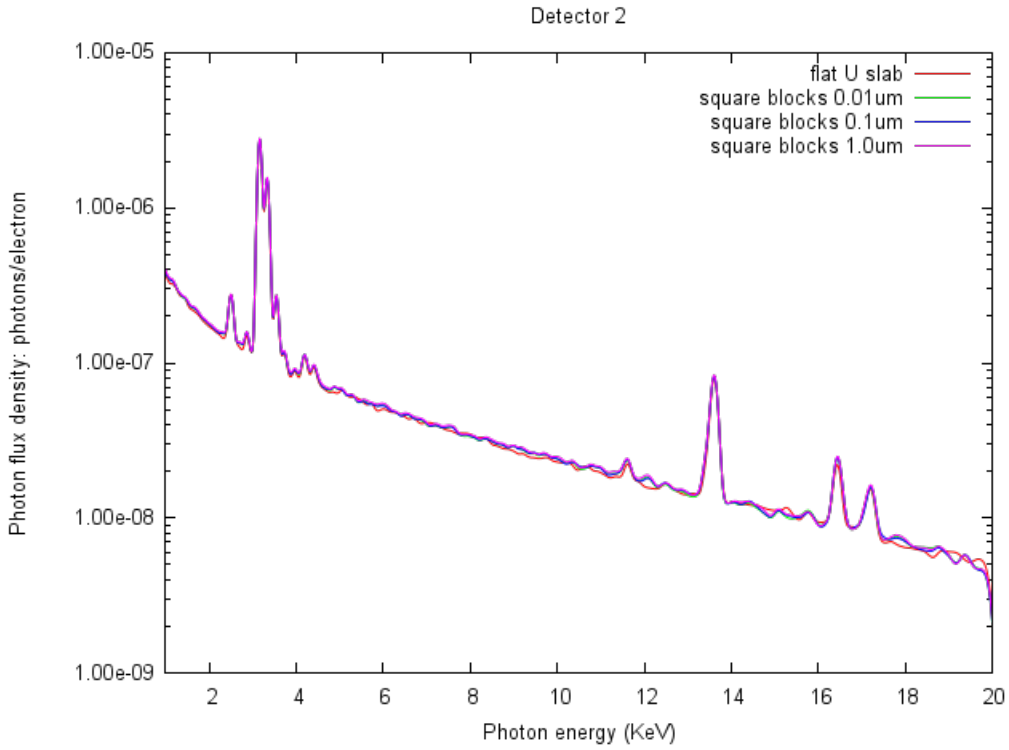

Figure 8. Surface geometry effects on detector 2 spectrum.

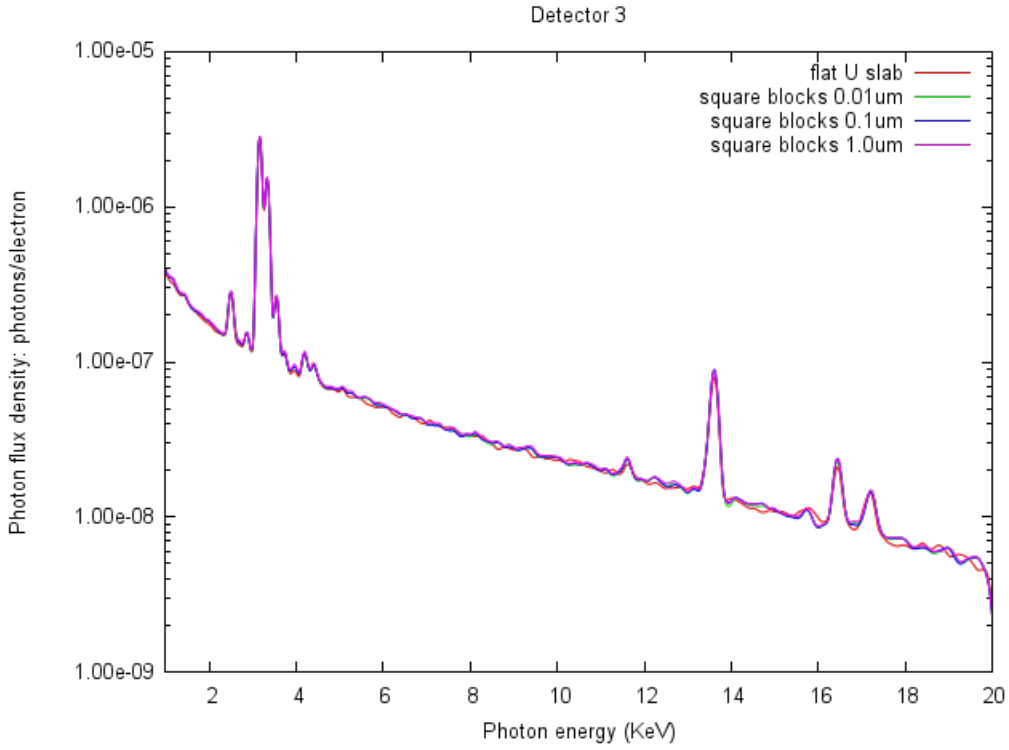

Figure 9. Surface geometry effects on detector 3 spectrum.

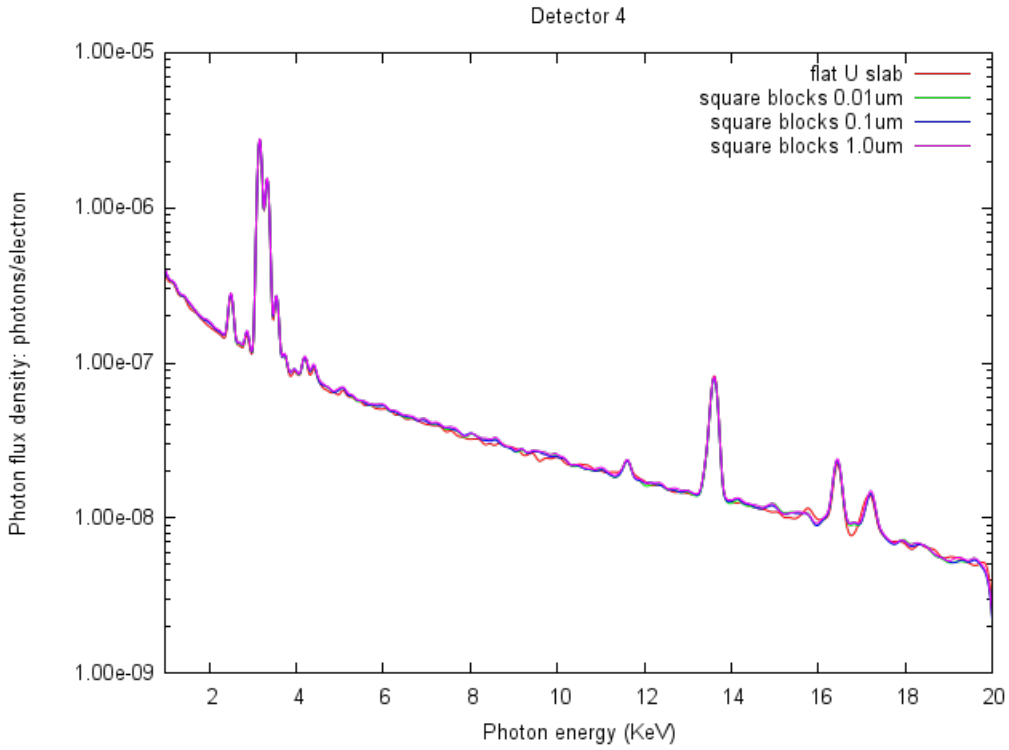

Figure 10. Surface geometry effects on detector 4 spectrum.

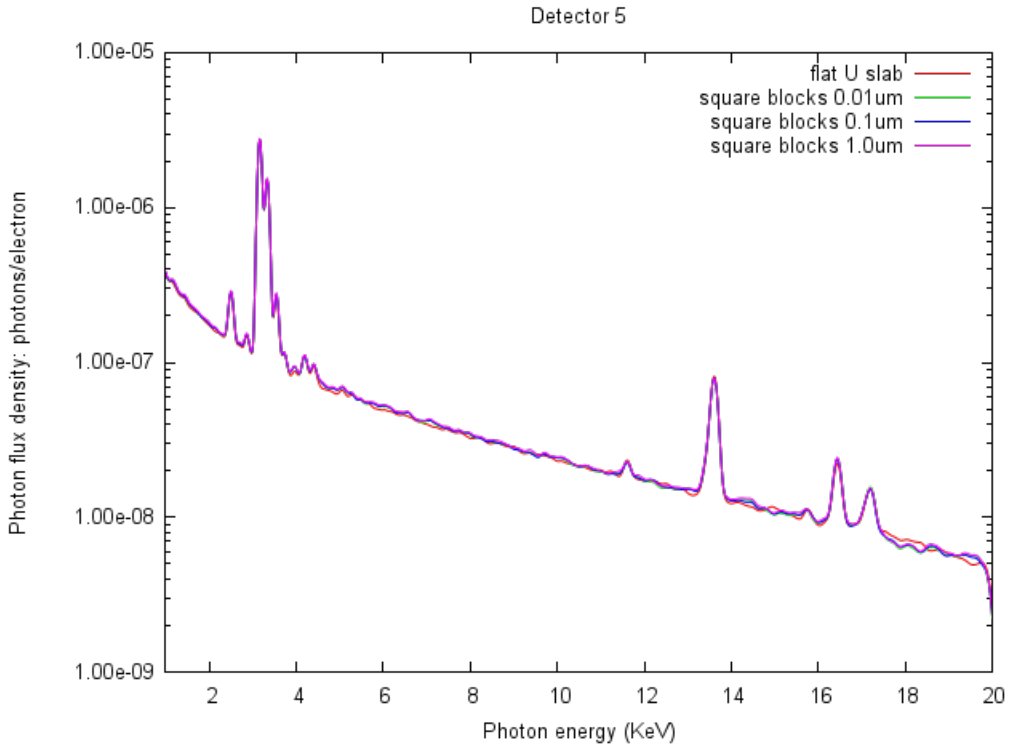

Figure 11. Surface geometry effects on detector 5 spectrum.

3.2. HETEROGENEITY TEST PROBLEM: ENVIRONMENTAL SAMPLING

A realistic heterogeneous problem is a mixture of particles consisting of heavy metals and mineral oxides embedded in some other material. A specific example is an environmental swipe sample, where the particles, embedded in soil, are collected on an organic substrate. The substrate material is the International Atomic Energy Agency (IAEA) reference swipe (TX-304) [6], and the swipe is assumed to rest on an aluminum sample holder. An illustration of the geometry of this proposed problem is shown below in Figure 12. The layer of the embedding medium is 5 microns thick. The initial radius of the spherical embedded particles is 1 micron. However, the radius and location of the particles in the embedding medium can be varied to quantitatively determine the sensitivity of the spectrum to these physical quantities. One micron was selected as the initial particle size since it was decided that this would be the minimum size to be encountered in a real analysis situation.

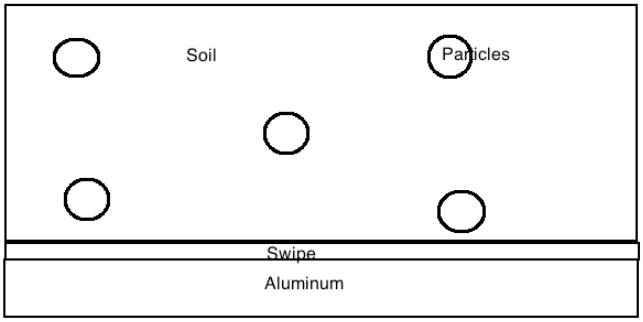

Figure 12. Model of IAEA swipe and embedding medium (not to scale).

Because of the small particle size, the beam interaction volume will likely include the particle, any embedding medium, and any substrate material. Thus, the spectral response will include the embedding and substrate medium as well as the properties of the particles themselves. Therefore, three different types of embedding media were evaluated, some without the organic swipe substrate, but all with the aluminum sample holder:

(1) soil with US average concentrations of potassium, uranium, and thorium (KUT) on an organic swipe material,
(2) polycarbonate without the organic swipe material, and
(3) nitrocellulose without the organic swipe material.

The polycarbonate and nitrocellulose are commonly used as media in SEM sample preparation, so they represent samples that have been prepared in the laboratory. Soil was considered as a typical medium that might be encounter from a raw IAEA swipe. The soil had impurities of potassium (K), uranium (U), and thorium (T)—commonly referred to as KUT content—with values of 370, 35, and 35 Bq/kg respectively, as encountered in average US soil. These values are taken from Table 5 of the 2000 United Nations Scientific Committee on the Effects of Atomic Radiation (UNSCEAR) Report [7]. The purpose of including the KUT impurities was to determine if they would mask the presence of any embedded uranium particles in the medium. It should be mentioned that the KUT content of soils varies quite dramatically worldwide. If the geographic location of the sample were known, it would be relatively easy to find an approximate KUT content for that locale and subtract the computational KUT portion of the spectrum from the total SEM spectrum. This is an example of how a computational SEM capability will have real world application, in that the response for different KUT contents of various soils can be computed in advance.

Figure 13 includes plots of the spectra simulated for the geometry in Figure 12, where the particles are soil (same as embedding medium), UO_2, UO_3, U_3O_8, and UO_2F_2. It can be seen from Figure 13 that the magnitudes of the uranium peaks in the soil-only geometry are less than the magnitudes generated from the embedded particles. If the number of embedded particles near the surface were lower, then of course the magnitude of the spectrum for the particles would move downward toward the soil spectrum and perhaps even be masked at the lower energies. However, the peak at approximately 13.8 keV is substantially higher than the soil level due to the low amounts of uranium in the soil and low cross section at this energy. This should serve as a prime indicator of the presence of non-naturally occurring radioactive material (non-NORM) uranium.

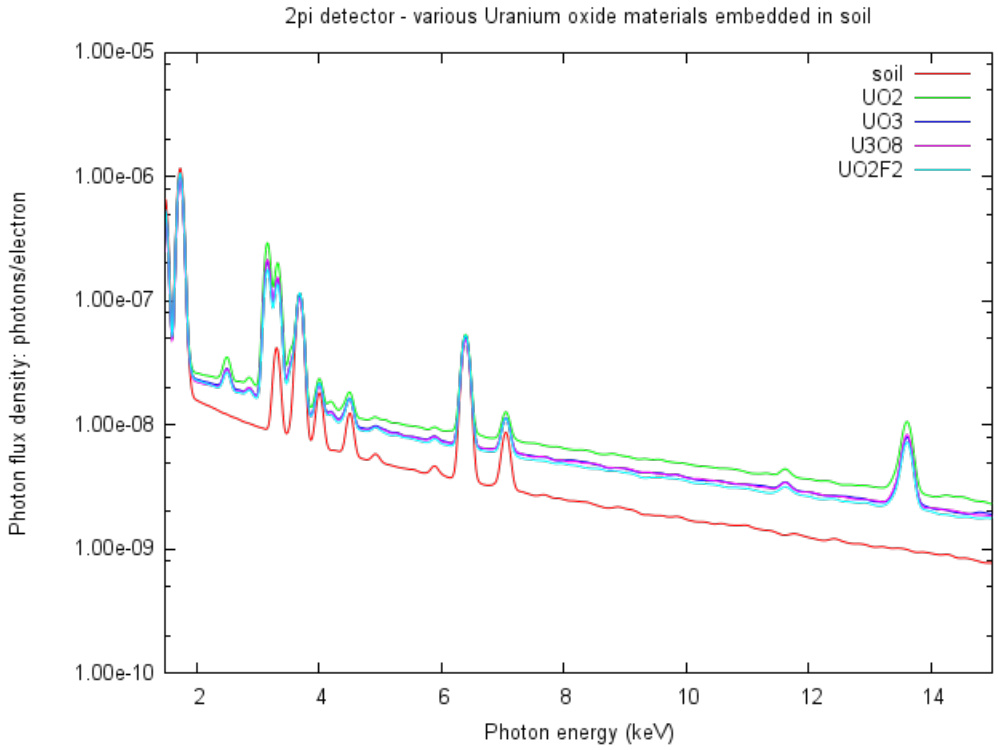

Figure 13. Spectrum sensitivity to soil medium.

3.2.1. Sensitivity to Embedding Medium

The results in Figure 13 used NORM-contaminated soil as the embedding medium. Typically, SEM samples are prepared using standard materials such as polycarbonate or nitrocellulose as the substrate. Polycarbonates are known by the trademarked names Lexan, arcoPlus, and other commercial names, and can produce molds that make them well suited for SEM sample mounting purposes.

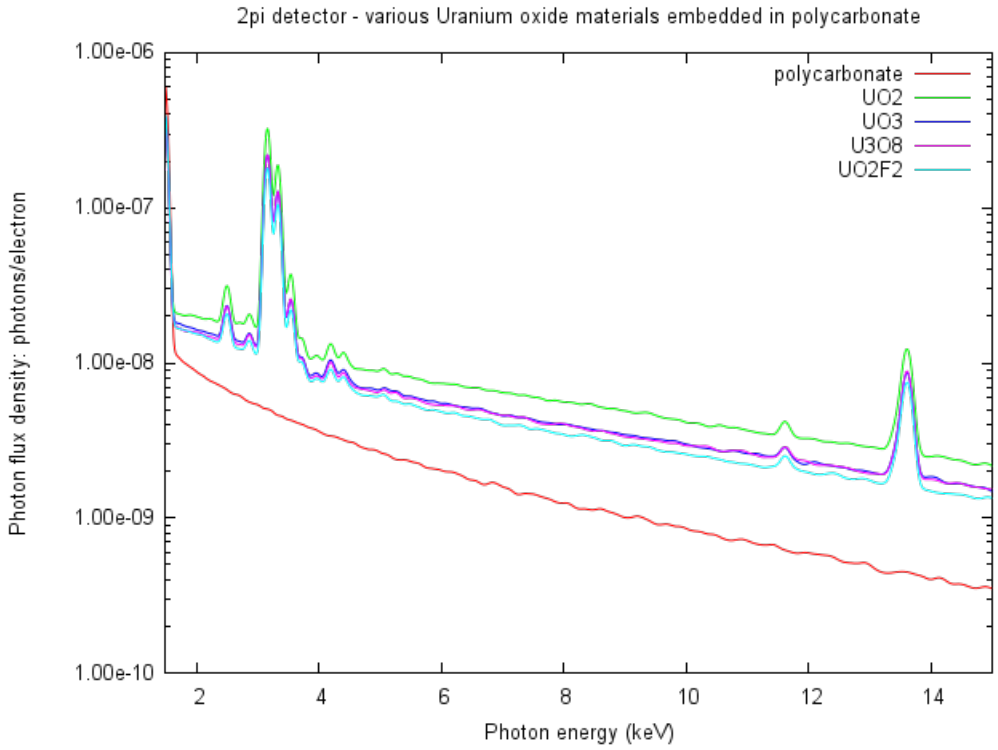

Figure 14. Spectrum sensitivity to polycarbonate medium.

Figure 14 shows the same embedded uranium particles in various oxide forms but with a polycarbonate medium in place of the soil. The most striking feature is the lack of structure or detail associated with the polycarbonate medium. This is very desirable, as this spectrum will pose little interference with the materials to be identified using the SEM x-ray spectra. Nitrocellulose has the chemical formula $C_6H_9(NO_2)O_5$ and is used as a film-forming polymer in certain specialty coatings for environmental samples. Figure 15 shows that the background of nitrocellulose is lower than soil similar to that of polycarbonate.

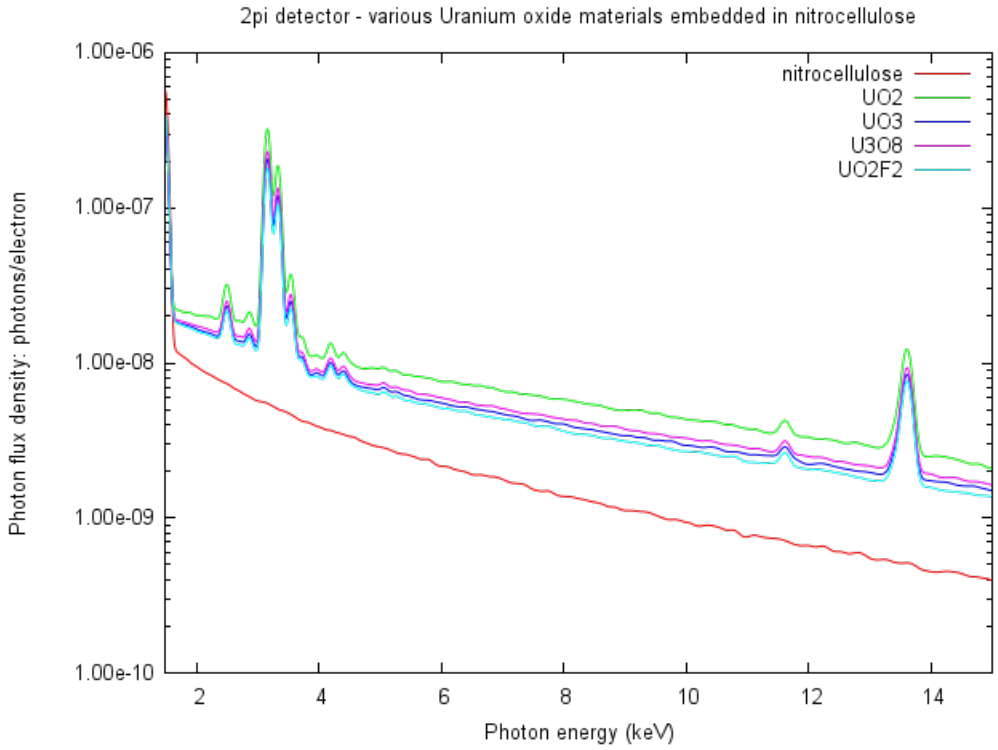

Figure 15. Spectrum sensitivity to nitrocellulose medium.

Thus, identification of SEM x-ray spectra and sample composition is not overly sensitive to the embedding and substrate materials. While well-prepared and smooth samples using polycarbonate or nitrocellulose will make for easier identification and accurate resolution of the photopeaks, a contaminated dirty sample does not appear to make the SEM technique infeasible for the identification of the embedded particles.

3.2.2. Sensitivity to Actinide Composition of Embedded Particles

While section 2.1 addresses the difficulty of distinguishing between different chemical compounds of the same actinide, the ability to distinguish between different actinides for the composition of the embedded particles is also a challenge. For this comparison, actinides in their basic oxide form (UO_2, PuO_2, and ThO_2) will be included in the Figure 12 geometry. The ability to distinguish between different actinides is of course a desired feature of any detection method.

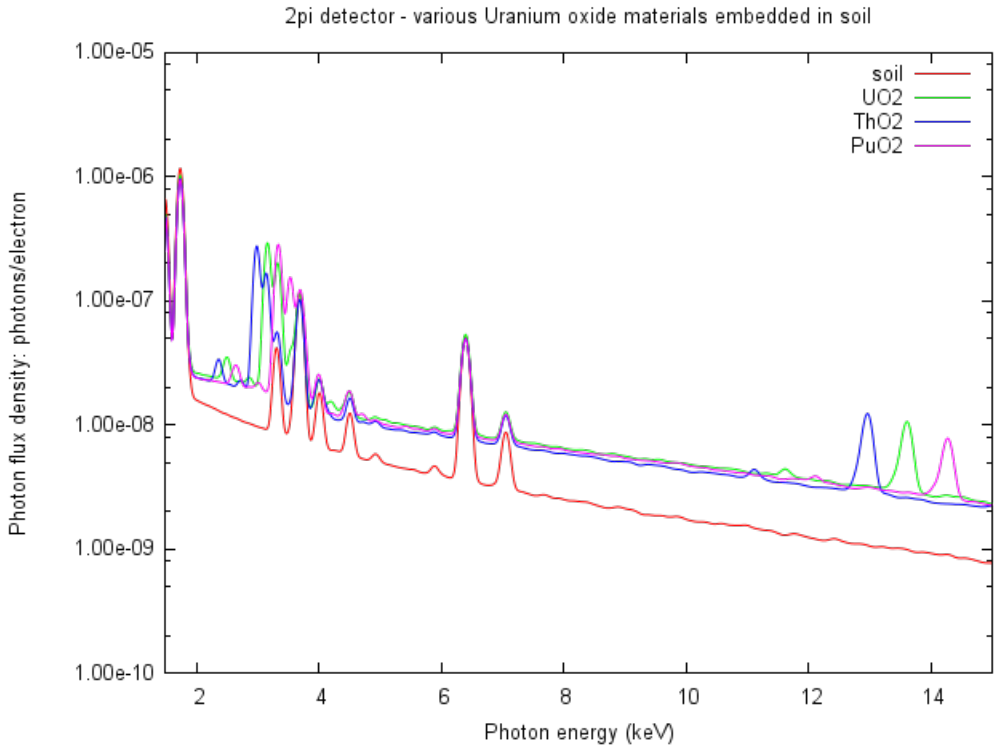

Figure 16. Spectrum sensitivity to different actinides.

Figure 16 shows the changes in the spectrum shape due to different oxides of uranium, thorium, and plutonium as the embedded particle form. SEM is clearly capable of distinguishing between different actinides, even in a NORM-contaminated soil medium.

3.2.3. Sensitivity to Size and Location of Material Heterogeneities

Another parameter of interest is the size and location of the embedded particles within the embedding medium. Figure 17 shows the change in the spectrum as the UO_2 particle size is increased but with the locations unchanged from Figure 12.

The magnitude of the spectrum is directly proportional to the size of the embedded particle. This is because the increase in particle size correlates to an increase in uranium content of the sample, which leads to an increase in the number of fluorescence x-rays produced within uranium atoms.

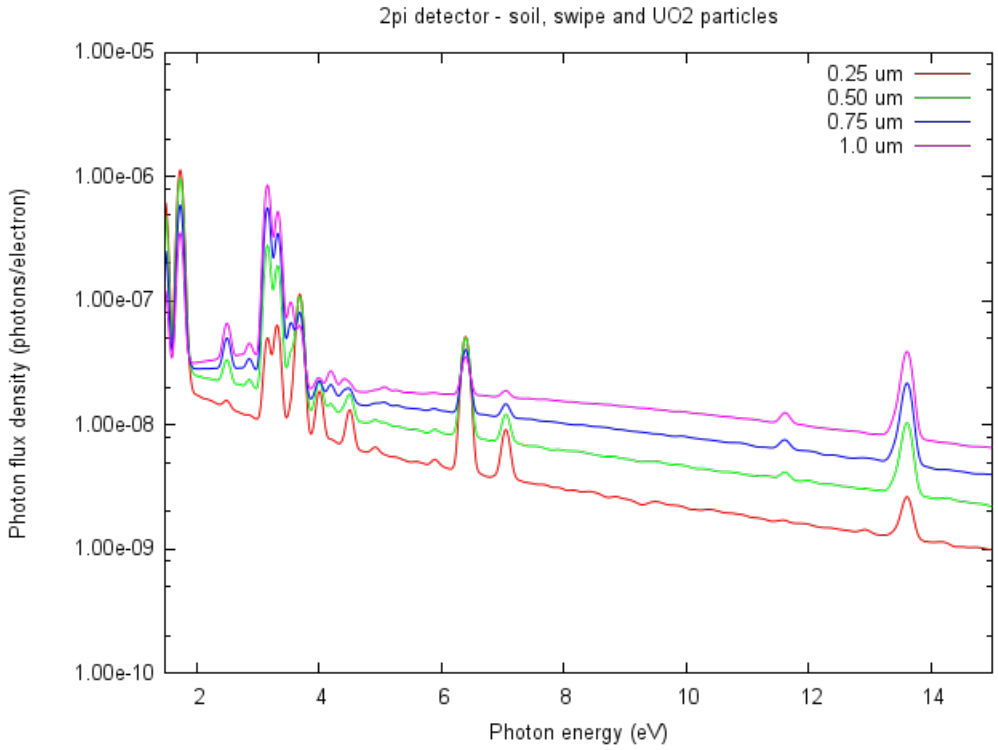

Figure 17. Spectrum sensitivity to embedded particle size.

An additional concern is the sensitivity of the spectrum to the embedded particle locations. Does bunching of the particles or layering particles near the sample surface cause any drastic changes in the response of the detector, either photon spectrum shape or magnitude?

Three different scenarios were developed to answer this question, all of which are perturbations of the Figure 12 geometry. The first case, known as "depleted central region," is illustrated in Figure 18. In this case, the central region is depleted of particles as the middlemost particle is moved downward into the second layer. This scenario will also give an indication of how much influence that particle had on the spectrum in Figure 13. If the electrons are not able to reach the deeper central particle of Figure 12, then the depleted central region case will show little or no change in magnitude over the Figure 12 geometry.

The second scenario is the "bunched central region" case, as depicted in Figure 19. In this case, the particles near the edges of the geometry are moved in closer towards the center, more tightly bunching the particles together. Note that the number of particles near the surface is unchanged.

The third scenario, presented in Figure 20, is the case of particles located in two layers near the surface, and is referred to as the "double layer."

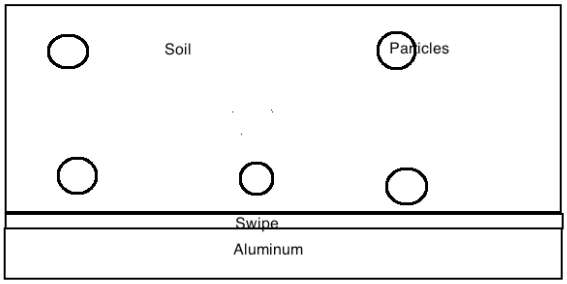

Figure 18. Particles depleted in central region (not to scale).

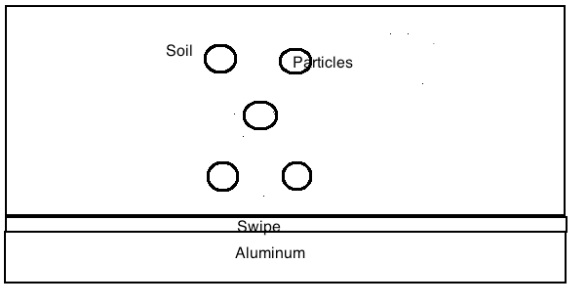

Figure 19. Particles bunched in central region (not to scale).

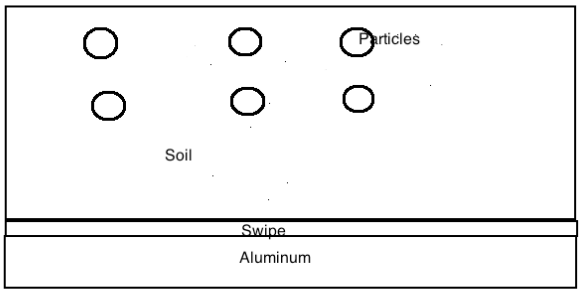

Figure 20. Double layer near surface (not to scale).

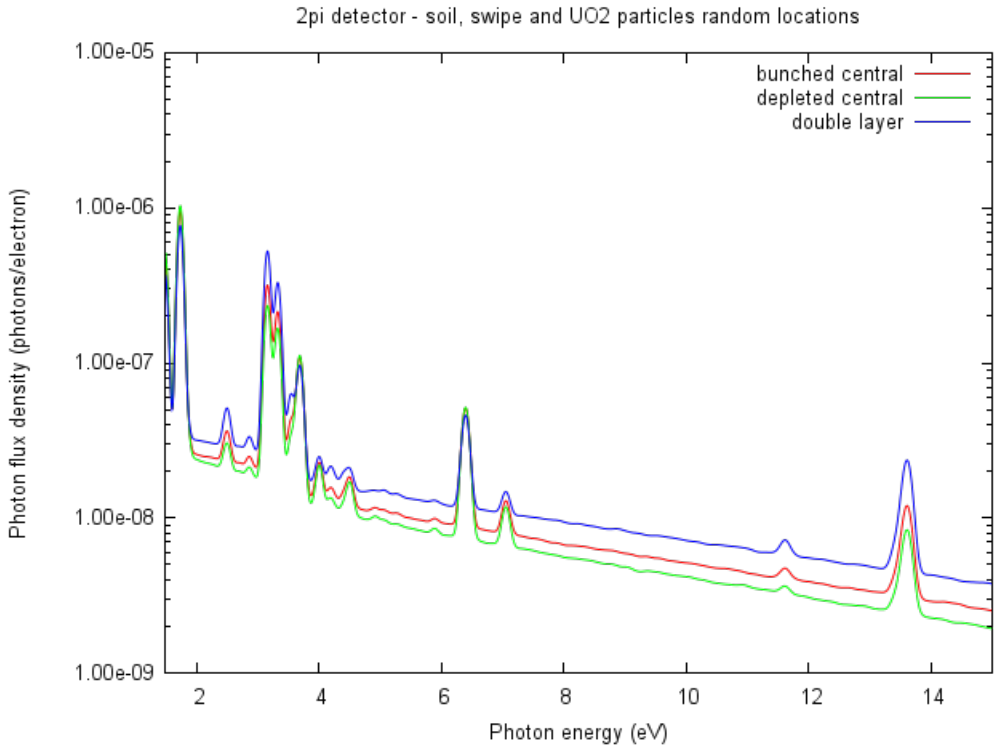

Figure 21. Spectrum sensitivity to particle locations.

Figure 21 shows that the spectrum shape is insensitive to the particle locations. Each of the three configurations has particles near the surface, and these particles are the main contributors to the x-ray spectrum. Note that the double layer case has more particles located near the surface and has the highest magnitude, which shows that particles near the surface have a greater effect on the spectrum. The bunched central region case is slightly lower since the overall number of particles near the surface is lower, and the depleted central region case has the lowest magnitude due to the lowest number of particles near the surface.

This illustrates one of the reasons for thin samples in SEM x-ray spectra measurements. For thick samples, the SEM electrons will not be able to penetrate deep into the sample and provide information about the interior. Thus, if the samples are thin enough that all the interior regions can be reached by the SEM electrons, the magnitude will be stable for different particle locations, as all the particles are being interrogated by the energetic electrons.

4. SUMMARY AND CONCLUSIONS

This sensitivity analysis provides some insight about which parameters will be impactful during an inverse simulation to determine the material composition based on a measured SEM spectrum. It has been shown that materials with very similar compositions can be distinguished, but this likely requires very small Monte Carlo statistical uncertainties, which corresponds to longer run times. Simulations below 1 keV are needed to identify materials with light elements. The parallel version of penORNL will help alleviate the simulation time concern. For samples that are larger than the interaction volume of the SEM electrons (approximately the range), mass density is not a major concern because there is little-to-no sensitivity to density for these large samples. The x-ray spectra are sensitive to the stopping power and electron shell transition probabilities, but they are more sensitive for the transition probabilities. Both of these parameters are data entered into the SEM Monte Carlo simulations and are not parameters that will be adjusted during the inverse analysis. However, uncertainties in this input data can impact the accuracy of the SEM Monte Carlo simulations and therefore the accuracy of the inverse analysis. Finally, the simulations of varying geometries/surface roughness and heterogeneity show there are no issues that would preclude the practical application of inverse methods to simulations of SEM x-ray spectra.

The next phase of this project will focus on determining the accuracy of composition predictions for simplified test problems using inverse techniques, which will progress to more complex test problems. A suggestion for future work following this project is (1) to determine the uncertainties of input parameters/basic data—like stopping power and electron shell transition probabilities—and (2) to propagate those uncertainties through to the Monte Carlo simulation results to assess their impact on the inverse simulations.

5. REFERENCES

1. T. M. Miller, C. F. Weber, and B. W. Patton, *Monte Carlo Simulations of X-ray Spectra from Scanning Electron Microscopes*, ORNL/LTR-2013/467, Oak Ridge National Laboratory, 2013.

2. T. M. Miller, C. F. Weber, and B. W. Patton, "Simulation of Electron Probe Microanalysis for the Purposes of Automated Material Identification—Initial Evaluation of Available Monte Carlo Tools," *Transactions of the American Nuclear Society*, **110**(1), p. 497 (2014).

3. F. Salvat, J. M. Fernandez-Varea, and J. Sempau, "PENELOPE, a code system for Monte Carlo simulation of electron and photon transport," Universitat de Barcelona (revised 2011).

4. C. F. Weber, K. B. Bekar, B. W. Patton, and T. M. Miller, *Simulation of SEM-EDS: Monte Carlo Code Development and Inverse Analysis*, ORNL/LTR-2014/557, Oak Ridge National Laboratory, 2014.

5. J. Goldstein, et. al., *Scanning Electron Microscopy and X-Ray Microanalysis*, Springer, New York, p. 63 (2003).

6. TexWipe Cotton Wipe®. https://texwipe.com/store/p-734-texwipe-cotton.aspx.

7. "Sources and Effects of Ionizing Radiation," UNSCEAR 2000 Report Volume 1, Appendix B.